Tomographic Velocity Determination of the Sedimentary and Salt Flank Images using Multifarious VSP data

Yingping Li*, VSFusion, A Baker Hughes-CGG Company, John O'Brien, Brian Mallick, Anadarko Petroleum Corporation, USA, Jie Zhang, GeoTomo, USA, Dapeng Wang, Celine Barberan, and David Dushman, VSFusion, A Baker Hughes-CGG Company

This paper was prepared for presentation at the 8th International Congress of The Brazilian Geophysical Society held in Rio de Janeiro, Brazil, 14-18 September 2003.

Abstract

This paper presents an application of seismic tomography to determine the velocity field on the flanks of a steep, deeply-buried salt body, enabling us to determine the configuration of the flank of the salt body. The method is applied to the Anadarko Tarantula #1 well drilled in the Gulf of Mexico, USA, in which an extensive VSP program was acquired. Data acquisition included one zero-offset VSP (ZVSP), two offset VSP (OVSP) surveys, a 3-D salt proximity (SP) survey, and a North-South walkaway VSP (WVSP), providing reasonably good ray coverage for tomographic analysis.

Arrival times of direct P waves and head waves propagating along the salt/sediment boundary were picked from 1118 seismic traces for tomographic inversion. The resulting velocity solution provides substantial detail on the velocity distribution within the sedimentary section and also provides clear definition of the salt/sediment interface. Identification of the salt boundary is consistent with the results of the salt proximity survey and provides independent corroboration of the salt flank location.

Introduction

Seismic tomography is a method for determining the subsurface velocity distribution from a multitude of seismic observations, such as VSP, cross-well, and surface seismic data. Tomography can provide valuable information about complicated geological structures and can generate a suitable velocity model for depth migration imaging. Stewart et al. (1987) applied tomography-based velocity modeling in VSP imaging. Salo and Schuster (1989) demonstrated traveltime tomography using VSP data. Zhou and Hou (2000) performed a reverse VSP tomographic velocity analysis. Zhang et al. (2001) developed a joint cross-well and VSP tomographic algorithm to image complex geological structures.

In this study, traveltime tomography was performed on a multifarious VSP dataset acquired at the Anadarko Tarantula #1 well. The setting for this extensive VSP/salt proximity survey is located at the Tarantula Field in South Timbalier Block 308 in the Gulf of Mexico, USA. The Tarantula #1 well was drilled vertically to 17,977 ft in 480 ft. water depth. Figure 1 shows the map view of the survey geometry and a north-south seismic section through the well. One of the objectives of the VSP survey was to delineate the steep salt flank and to resolve interpretation ambiguities of the salt flank on 3-D surface seismic data. The salt flank location estimated from the salt proximity survey (Figure 1) and VSP depth migration has been published by O'Brien et al. (2002).

The objectives of this study are 1) to determine the configuration of the salt flank using VSP tomography and compare this with the results of the salt proximity survey; 2) to generate a velocity model with lateral heterogeneity that can be used to improve the VSP depth migration imaging. Tomography should complement the previous studies (O'Brien at al, 2002) on the shape of the salt flank and provide new information about the complex velocity structures in the area. The results from this study can be integrated with other data to assist in the interpretation of the subsurface structure.

Method

The traveltime data, T, can be written as a non-linear function, F, of the velocity model, m,

$$T = F(m). \quad (1)$$

The goal of tomographic inversion is to find a model (m) which exhibits the formation characteristics and can reproduce the traveltime data (T). An objective function, O, (Cheng & Zhang, 2001) is defined as:

$$O = ||T^{obs}-F(m)||^2 + \beta(\alpha||D_1C^{-1}(m)||^2+||D_2C^{-1}(m)||^2), \quad (2)$$

where T^{obs} is the data, $F(m)$ is the model predicted data, D_1 and D_2 are the first and second order directional derivative operators, respectively, $C^{-1}(m)$ is the model covariance matrix, α is the relative coefficient of the first order derivative, and β is a smoothing parameter. The non-linear inversion problem is solved using an iterative conjugate gradient method.

An additional term in the object function for the non-linear tomography helps to preserve the sharp changes associated with the interfaces in the velocity field. This inversion scheme has particular merit here as the sediment-salt boundary has a large velocity contrast. An improved version of the shortest path raytracing (SPR) algorithm (Zhang & Toksoz, 1998) was used to calculate traveltimes. This is a wavefront based algorithm that handles refractions and diffractions more accurately than conventional bending or shooting algorithms.

Data, Inversion, and Results

The VSP waveform data used in this study are shown in Figure 2. This dataset consists of the following:

1. A 236-level zero-offset VSP,
2. Two 128-level offset VSPs with the seismic source locations at 2000 and 4000 ft. south of the well,
3. A 71-level salt proximity survey at an offset location of 12,800 ft, and
4. A five-level walkaway VSP with 111 shots, ranging from -5981 (north) to 16002 ft (south) with shotpoint interval of 200 ft.

Geophone depth intervals were 50 ft for the VSP and 100 ft for the salt proximity survey.

A non-linear tomography code, TOMOXPRO, was employed to determine the subsurface velocity field. Processing steps include arrival time picking, generating the initial velocity model, and tomographic inversion. 3-component rotation was performed on the VSP data using an eigenvalue rotation technique in order to maximize the arrival energy in the direct component. The first break times (FBT) of P waves were initially picked on the vertical component and refined subsequently using the direct component wavelet (red marks, Figure 2). To constrain the background velocity distribution of the sedimentary rocks, the first sediment arrival times (FSAT) were also picked (pink lines, Figure 2).

Figure 3 shows the initial flat planar velocity model, which was built based on the zero offset VSP time/depth pairs, and a tomographic velocity inversion using the first break times (FBT) after 20 iterations. The resulting solution shows a high velocity (~15000 ft/s) region which roughly defines the salt-sediment boundary. However, the sediment velocity distribution indicates that the flat layer model is incorrect and suggests the initial velocity model should be refined to include dipping sediment structures and information about the salt top.

A more complex sediment velocity model with dipping structures (Figure 4a) was built, based on interval velocity data from the zero offset VSP survey and structural dips from the surface seismic data. A tomographic image of the sediment velocity distribution was obtained by inverting the FSAT data for 14 iterations (Figure 4b). Significant lateral variations within the layers can be observed, with minor differences in the major interfaces.

A salt body was added to the resulting background sediment model in Figure 4b to create an initial salt-sediment model (S-S Model 1, Figure 4c). Tomographic inversion was performed with the first break times (FBT) and S-S Model 1 as the starting model. The tomographic solution obtained after 50 iterations is displayed in Figure 4d. The pink zone with a high velocity (~15000 ft/s) in the reconstructed velocity model clearly delineates the shape of the salt flank (Figure 4d). The reconstructed velocity model also shows the updip sediment layers next to the steep salt flank.

To test the effects of initial models on the final tomographic velocity field, we carried out the FBT tomographic inversion with a different initial velocity model (S-S model 2) which had a different shape for the salt body (Figure 4e). The solution is displayed in Figure 4f. Despite using two different starting sediment-salt models the final profiles for the steep portion of the salt flank (Figures 4d and 4f) are almost identical.

Seismic ray paths were calculated using a wavefront algorithm (Zhang & Toksoz, 1998) for two final velocity models and were superimposed on the two tomographic velocity profiles (Figure 5), showing ray coverage for the inversions. The best ray coverage occurs at the steep salt flank and sediments in that vicinity where the two final tomographic images agree well with each other (Figures 4d and 4f). There are some slight differences between the solutions at places of poor ray coverage such as the less steep portion of the salt flank and sediments above it (Figures 4d, 4f and 5).

Figure 6a displays the RMS errors as a function of the number of iterations with four different initial velocity models. The tomographic inversion with the flat initial model and the FBT (Figures 3a and 3b), shows the RMS misfits decrease monotonically from 294.3 ms to 31.7 ms after 19 iterations and then slightly increase to 33.1 ms. Although the velocity field shows an interface that seems to be a salt boundary (Figure 3b), the sediment velocity structures appear to be imprecise with such a large error. Integrating the zero offset VSP velocities and surface seismic information, a complex sediment velocity model with dipping structures was built. After 14 iterations, the RMS misfit decreases from 28.1 ms to 7.6 ms for tomographic inversion with the complex model and the FSAT, indicating that the complex model is a suitable background velocity model for the sedimentary rocks. The RMS errors for the tomographic inversion with the FBT and two sediment-salt models (S-S Model 1 and S-S Model 2 in Figures 4c and 4e) reduce the errors to 7.8 and 6.9 ms, respectively, after 50 iterations.

The key results of this study are displayed in Figure 6b. The tomographic velocity field obtained by inverting the first break times with an initial model clearly defines the steep salt flank and shows the velocity distribution of the sedimentary rocks flanking the salt edifice. The shape of salt flank closely matches the salt face determined by the salt proximity survey (Figure 6b). The success of the tomographic solution is due to having a well constrained complex sediment velocity model, which was obtained by inverting the sediment first arrival times. The tomographic velocity field reveals significant lateral heterogeneity in the sediments.

O'Brien et al. (2002) performed Kirchhoff depth migration of the salt flank P reflection using a simple sediment velocity model and compared the result with the salt proximity result. It was found that the two gave consistent dip estimates but differed in absolute value by up to 500 ft. These differences were attributed to 3-D effects which affect the reflection data. In addition to the 3-D effects, a relatively simpler velocity model may also have contributed to such differences. The complex velocity model derived from this tomographic inversion should improve the VSP depth migration image.

Conclusions

It has been demonstrated that a multifarious VSP dataset can be successfully used to produce tomographic velocity profiles of complex sediment structures and to the shape

of a steep salt flank. The first sediment arrival times (FSAT) were inverted to obtain a background velocity distribution of sedimentary rocks. Tomographic inversion of the first break times (FBT) clearly defines the salt boundary and refines the sediment structures with laterally varying velocities. The tomographic solution provides a validation of the salt proximity result and yields an increased sense of confidence in the location of the steep salt flank. A reliable sediment velocity model will subsequently improve the depth migration of the salt flank reflection. The VSP tomographic velocity field, VSP depth migration, salt proximity results, and surface seismic data can be integrated to characterize the salt flank with a high degree of confidence in a complex geological setting.

Acknowledgments

We would like to thank Anadarko Petroleum Corporation for giving permission to publish this work and to Baker Hughes Inc. for supporting this study. The seismic data are reproduced courtesy of PGS/Diamond Geophysical. Thanks Fran Doherty and Ran Zhou for reviewing this paper and providing constructive comments.

References

Cheng, A. C. H. and Zhang , J., 2001, Imaging complex structures with crosswell Seismology: SEG International Meeting, San Antonio, TX, In CD-ROM.

O'Brien, J., Mallick, B., Lakings, J., and Barberan, C., 2002, Locating the Salt Flank using Borehole Seismic Techniques: SEG International Meeting, Salt Lake City, UT, In CD-ROM.

Salo, E.L., and Schuster, G.T., 1989, Traveltime inversion of both direct and reflected arrivals in vertical seismic profile data: Geophysics, Vol. 54, p49-56.

Stewart, R.R., Chiu, S.K.L., Wilcox, M.A., and Hampson, D.P., 1987, Tomography-based imaging using well logs, VSP, and 3D seismic data: 57th Ann. Internat. Mtg., Soc. Expl. Geophys., Expanded Abstracts, p849-851.

Zhang, J., and Toksoz, M.N., 1998, Nonlinear refraction traveltime tomography: Geophysics, Vol. 63, p1726-1737.

Zhang, Z., Jackson, J., and Zhang, J., 2001, Reconstruction of high-resolution velocity models using joint tomography of crosswell and VSP data: Geophysics, 63rd EAGE Expanded Abstract, In CD-ROM.

Zhou, H., and Hou, A., 2000, A reversed VSP tomographic velocity analysis: 70th Ann. Internat. Mtg., Soc. Expl. Geophys., Expanded Abstracts, p1771-1774.

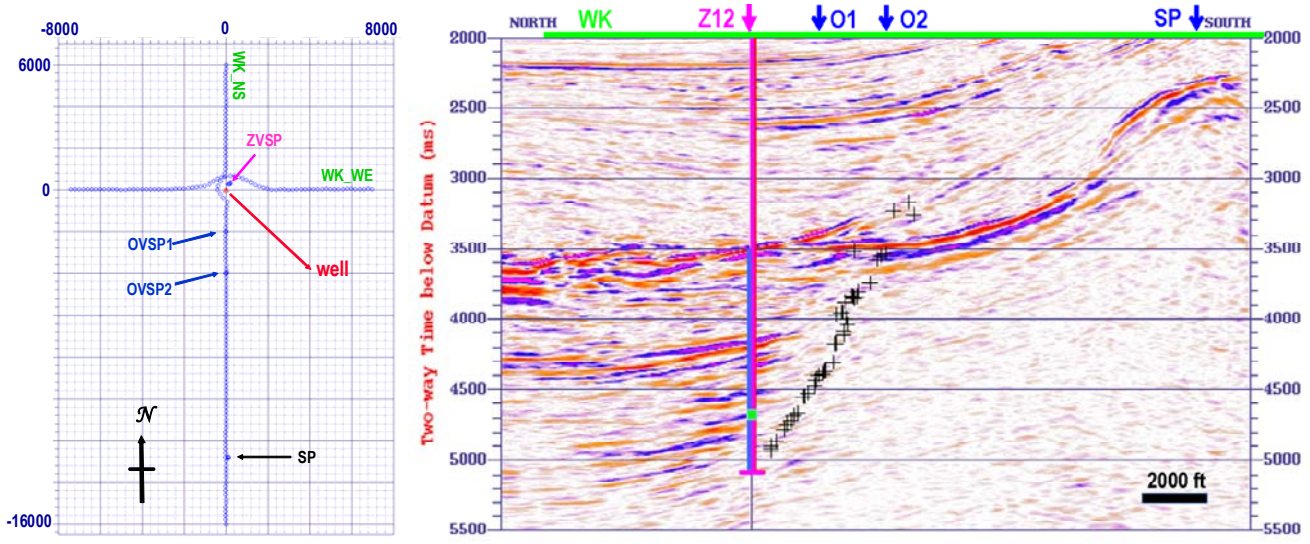

Figure 1 – Map view of VSP survey configuration (left) and surface seismic cross-section (North-South) showing structure, well position, and VSP energy source positions (right). Salt exit points (black +) obtained from the salt proximity survey (SP) are superimposed on the North-South surface seismic profile.

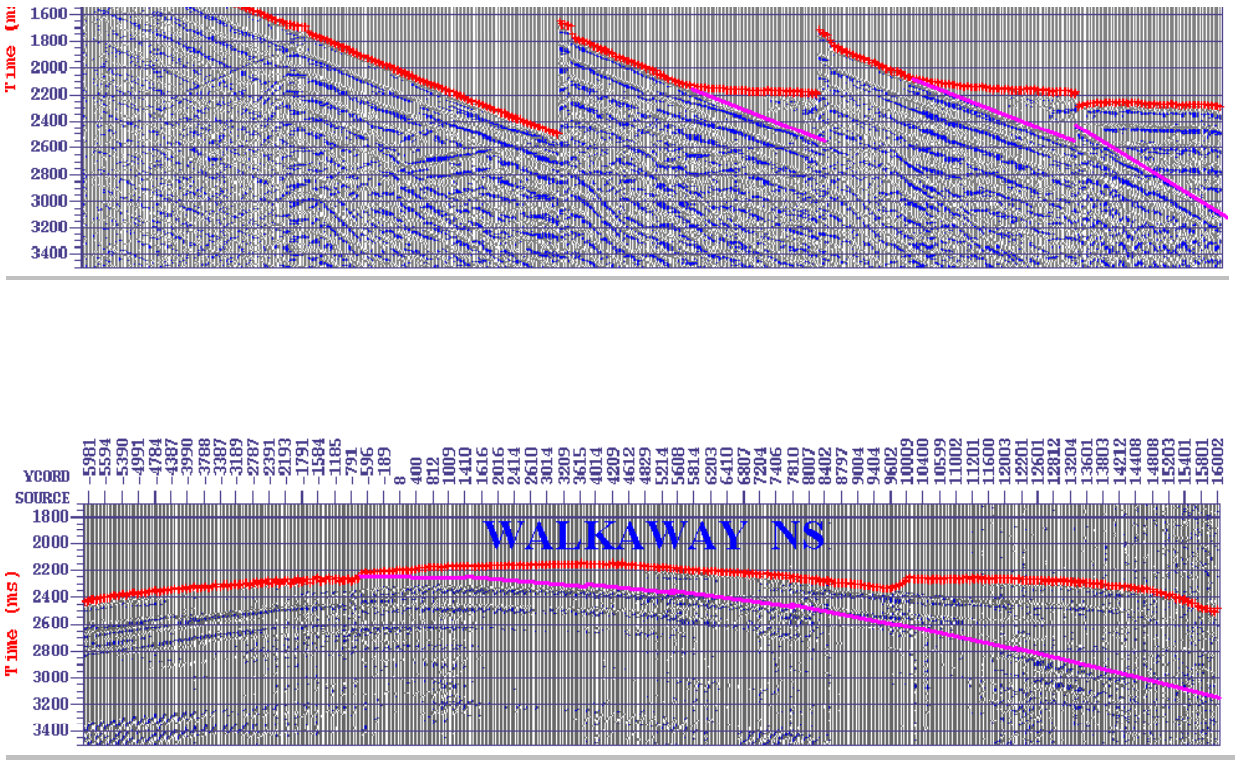

Figure 2 – Seismic traces from a multifarious VSP survey. Top: zero offset VSP offset VSPs, and salt proximity survey. Bottom: walkaway VSP. Red lines are the first break time (FBT) picks and pink lines represent picks for the first sediment arrival times (FSAT).

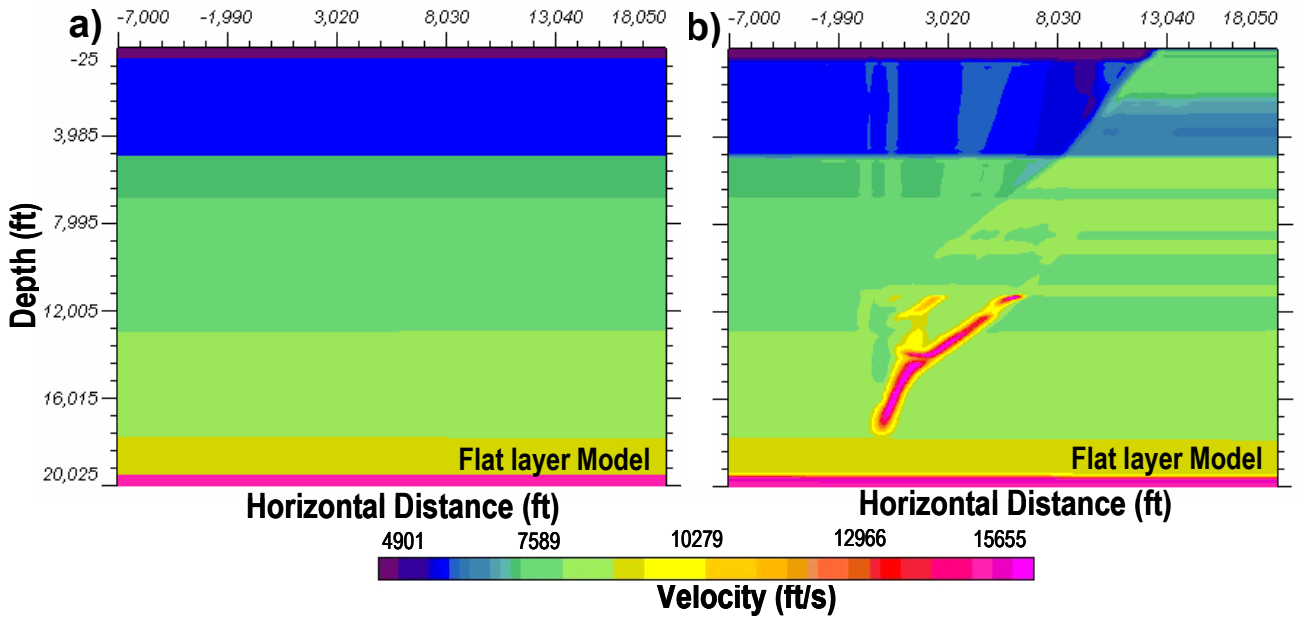

Figure 3 – a) An initial, flat layer velocity model for tomography built using the zero-offset VSP data. b) A reconstructed model from tomography using the first break times (FBT) of a multifarious VSP dataset.

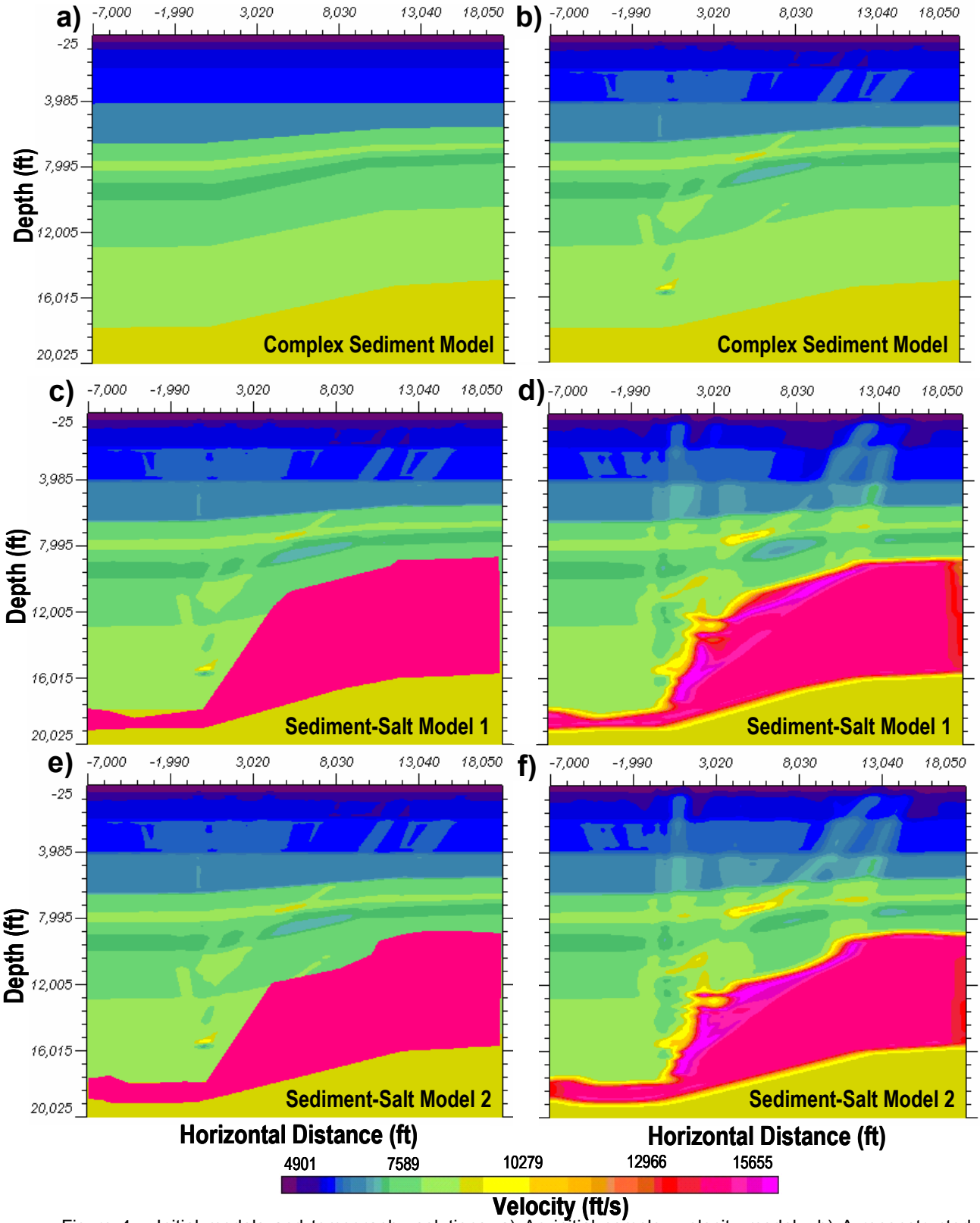

Figure 4 – Initial models and tomography solutions. a) An initial complex velocity model. b) A reconstructed sediment model from tomography inversion with FSAT. c) A salt body was built on the complex sediment model and used as an initial model for tomography inversion. d) A reconstructed model from VSP tomography with FBT. e) Initial model with a different salt shape. f) A tomography image reconstructed using model in e) as an initial model.

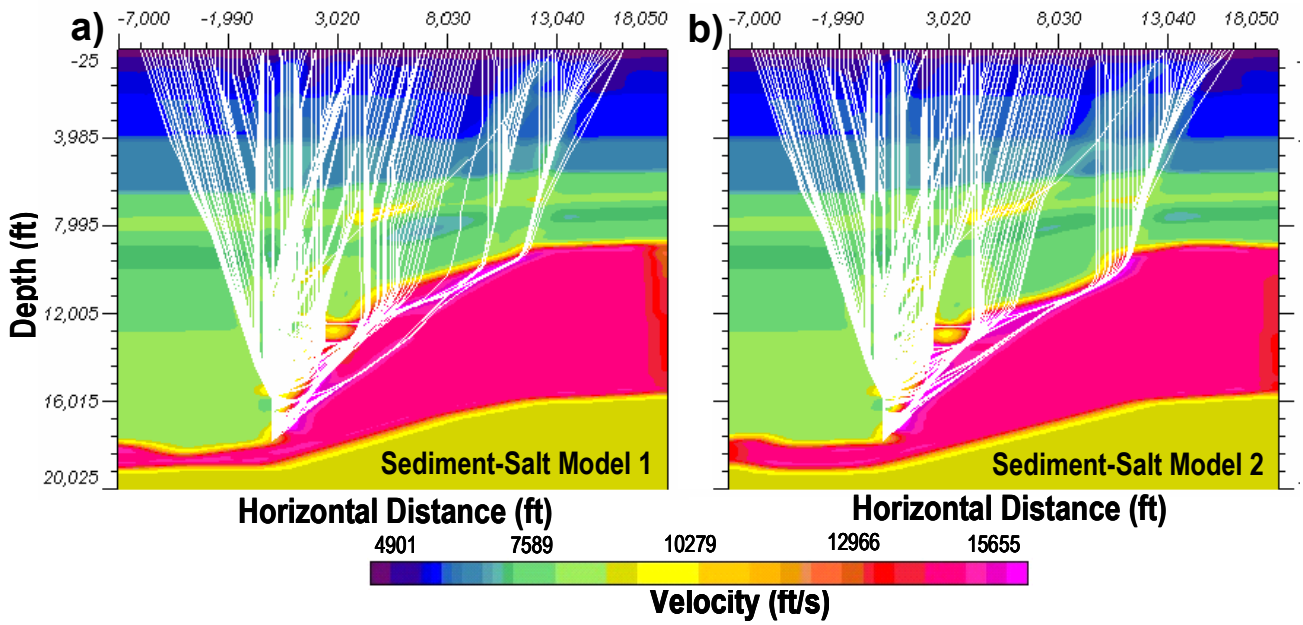

Figure 5 - Seismic ray paths, superimposed on two reconstructed velocity models, show the ray coverage for two tomography inversions for a) Sediment-Salt Model 1 and b) Sediment-Salt Model 2.

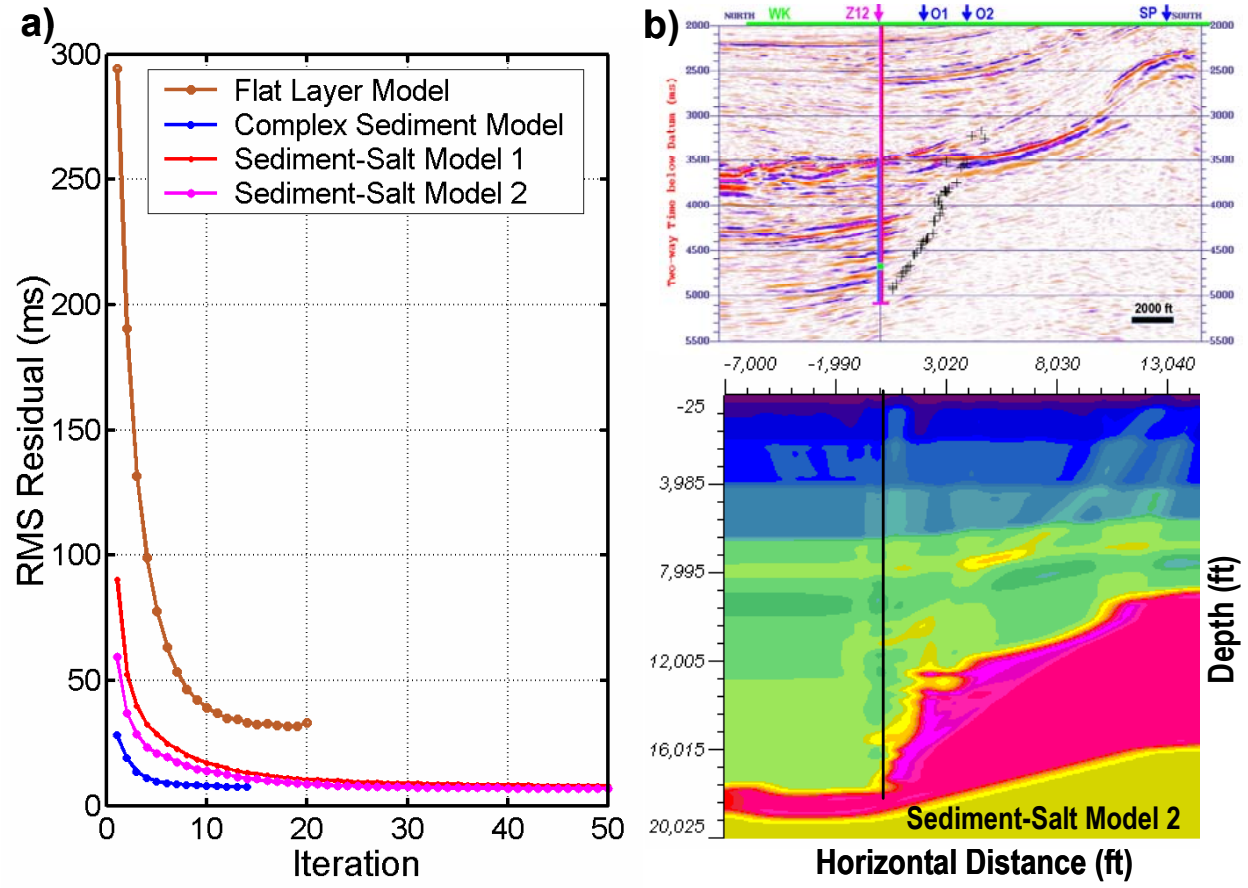

Figure 6 – a) Comparison of RMS residuals for four tomography inversions. b) Surface seismic profile and salt exit points versus the final VSP tomography velocity field using the first break times (FBT).